

Reconfigurable Intelligent Surfaces Empowered THz Communication in LEO Satellite Networks

Kürşat Tekbıyık, *Graduate Student Member, IEEE*, Güneş Karabulut Kurt, *Senior Member, IEEE*,
Ali Rıza Ekti, *Senior Member, IEEE*, Halim Yanikomeroglu, *Fellow, IEEE*

Abstract—The revolution in the low Earth orbit (LEO) satellite networks will bring changes on their communication models and a shift from the classical bent-pipe architectures to more sophisticated networking platforms. Thanks to technological advancements in microelectronics and micro-systems, the terahertz (THz) band has emerged as a strong candidate for inter-satellite links (ISLs) due to its promise of high data rates. Yet, the propagation conditions of the THz band need to be properly modeled and controlled with utilizing reconfigurable intelligent surfaces (RISs) to leverage their full potential. In this work, we first provide an assessment of the use of the THz band for ISLs, and quantify the impact of misalignment fading on error performance. Then, in order to compensate for the high path loss associated with high carrier frequencies, and to further improve the signal-to-noise ratio (SNR), we propose the use of RISs mounted on neighboring satellites to enable signal propagation. Based on a mathematical analysis of the problem, we present the error rate expressions for RIS-assisted ISLs with misalignment fading. Also, numerical results show that RIS can leverage the error rate performance and achievable capacity of THz ISLs.

Index Terms—Inter-satellite links (ISLs), low Earth orbit (LEO) satellite networks, terahertz (THz) band, reconfigurable intelligent surfaces (RISs).

I. INTRODUCTION

Thanks to recent advances in space technology, satellite production and deployment costs have been significantly reduced. As a result, low Earth orbit (LEO) satellites have become an attractive option for providing ubiquitous and low-latency communications [1]. The unprecedented growth in LEO satellite deployments has opened new horizons for the wireless communication world. For example, SpaceX, which plans to launch thousands of satellites in LEO and lower orbits to cover the vast majority of the users, aims for seamless and low latency communication between satellites [2]. To provide ubiquitous and flexible connectivity solutions, new types of satellites supporting cooperation between satellites and multi-band support are needed. Furthermore, it is envisioned that

small satellites will be key drivers for space communications owing to low production and deployment costs associated with launching a satellite into orbit [3]. The satellite networks seem to include a massive number of satellites and CubeSats. For example, SpaceX is planning to deploy 1600 satellites for Starlink’s initial phase and SpaceX additionally proposes launching extra 7518 satellites into the orbit with an altitude of 340 km [4]. A cooperative communication paradigm seems to be appropriate for more efficient and effective use of a network with such a large number of satellites. Therefore, the requirements for satellite communications need to be revised and redefined to suit small satellites with relatively low power transmission capacities. As the state-of-art technology, the terahertz (THz) band has emerged as a promising solution for inter-satellite links (ISLs) since it can provide high-data-rate communications due to its untapped wide bandwidth [5, 6]. However, THz waves suffer from severe path loss [7, 8]. Fortunately, path-loss due to molecular absorption is a non-issue for space applications of THz communications. Nevertheless, misalignment between transmitter and receiver antennas can dramatically decrease received power, as shown in [9, 10] due to their narrow beams and high directivity.

Furthermore, taking the transmission power limits of LEO satellites into account, energy-efficient communications involving THz links can be met by using software controlled surfaces [11]. In a recent study, transmission through reconfigurable intelligent surfaces (RISs) was proposed as a novel communication technology with considerable potential [12]. The RISs with a massive number of passive elements on a flat surface can manipulate the propagation medium by separately adjusting the phase of impinging signal by each element of RIS. The main advantage of the RISs is the lack of active elements, which consume power, while Multiple-input multiple-output (MIMO) and relay-based communication systems employ several active elements. The passive reflectarrays and phased arrays have been already employed in satellite communication systems to indemnify the path loss through the long propagation distance. But, it should be noted that reflectarrays are not capable to adaptively adjust the characteristics of the impinging signal. On the other hand, RISs can adaptively change beamforming direction and eliminate multipath effects [13]. Furthermore, the RISs do not need complex processing or coding [14]. In this respect, these appealing features make RISs prominent to improve the communication performance and quality of service (QoS) for small satellites with low power consumption requirements. As detailed in [15], RISs can provide energy efficiency for the

K. Tekbıyık is with the Department of Electronics and Communications Engineering, İstanbul Technical University, İstanbul, Turkey, e-mail: tekbiyik@itu.edu.tr

G. Karabulut Kurt is with the Poly-Grames Research Center, Department of Electrical Engineering, Polytechnique Montréal, Montréal, Canada, e-mail: gunes.kurt@polymtl.ca

A.R. Ekti is with the Grid Communications and Security Group, Electrification and Energy Infrastructure Division, Oak Ridge National Laboratory, Oak Ridge, TN, U.S.A., e-mail: ektia@ornl.gov. This manuscript has been authored in part by UT-Battelle, LLC, under contract DE-AC05-00OR22725 with the US Department of Energy (DOE). The publisher acknowledges the US government license to provide public access under the DOE Public Access Plan (<http://energy.gov/downloads/doe-public-access-plan>).

H. Yanikomeroglu is with the Department of Systems and Computer Engineering, Carleton University, Ottawa, Canada, e-mail: halim@sce.carleton.ca

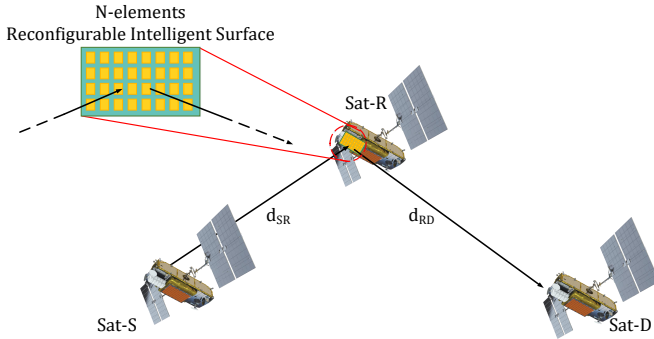


Fig. 1: The system model of an RIS-empowered ISL. The distance between the source (Sat-S) and the relay (Sat-R) is d_{SR} . Sat-R is equipped with an RIS that is composed of N elements. The distance between the relay and the destination (Sat-D) is d_{RD} .

same QoS level. RISs are expected to be a key enabler for THz waves in small satellites of the future [16] due to the energy efficiency [17] and low hardware complexity [18] provided by RISs. In [19], an architecture for RIS-assisted LEO satellite communications with RISs deployed at satellite and ground nodes and cooperative passive beamforming are proposed. The authors jointly optimize both beamforming at satellite and ground nodes to maximize the channel gain between satellite and ground nodes. But, the misalignment fading is not considered in that study.

In this study, we investigate RIS-assisted THz band ISLs in LEO constellations, as depicted in Fig. 1, to meet the requirements such as low-latency, ubiquitous connectivity, high data rates, and low-complexity. Moreover, RISs can allow flexibility in the direction of transmission, which is originally restricted to four nearby satellites in Starlink constellations [20]. Taking the above into account, we propose a cooperation between RIS-assisted satellites within the same and nearby orbits, and we derive error performance expressions to assess the potential of cooperative techniques in RIS-assisted THz ISLs. The expressions we derive are then validated with simulation results. Considering the relative motion and changing distance between satellites in different orbits, the performance analyses are carried out for the upper and lower limits by setting the closest and furthest possible distances.

A. Contributions

The use of an RIS-empowered THz band in LEO satellite ISLs is a promising tool to address high power consumption and low diversity order problems of a single ISL. The contributions of this study are summarized here:

Contribution 1: The utilization of RIS in THz communication systems is proposed. This enables the efficient transmission of the THz waves, which suffer from high path loss. As shown in [21], the effective path loss exponent can be reduced by the use of RISs in wireless communication links. To the best of our knowledge, this study is the first to provide an error performance analysis for RIS-assisted THz ISLs in LEO satellite networks.

TABLE I: The distances for Iridium and Starlink constellations.

| Specifications | Iridium | Starlink ¹ |
|----------------------------|---------------|-----------------------|
| r_s (km) | 781 | 1150 |
| N_{sat} | 11 | 50 |
| N_{orbit} | 6 | 32 |
| θ | 32.73° | 7.2° |
| Ψ | 30° | 5.625° |
| d_{intra} (km) | 4034 | 945.4 |
| d_{nearest} (km) | 2037.8 | 472.93 |
| d_{farthest} (km) | 4162.8 | 876.57 |

Contribution 2: First, we focus on the single RIS-assisted THz ISLs to enhance the power efficiency of the LEO satellite networks, as well as to improve the achievable data rates. The authors consider the misalignment fading, which will be observed in high velocity satellite systems utilizing narrow THz beams, in the performance analysis. To the best of our knowledge, this study is the first to consider the misalignment fading in RIS-assisted communications.

Contribution 3: We address the utilization of RIS-assisted THz satellite networks in a cooperative manner in this study. The benefit of multiple satellites' cooperation is shown to enhance power efficiency for a constant bit error probability.

Contribution 4: Considering Starlink and Iridium as two sample systems, the performance analysis is carried out in deference to their specifications given in Table I. Thus, the performance results regarding the cases that Starlink and Iridium satellite networks employ the proposed communication framework which utilizes RISs and THz signaling in ISLs are revealed.

B. Outline

The rest of this paper is organized as follows. In Section II, we introduce the associated model of the ISLs in LEO constellations in which intra-plane and inter-plane distance models are overviewed. The communication model of the RIS-assisted THz ISL links is given in Section III along with the misalignment fading model. Also in this section, single RIS-assisted and multiple RIS-assisted communication scenarios are considered, and the associated error expressions are derived. Extensive numerical results and observations are presented in Section IV including for both single and multiple RIS aided cooperation scenarios. In Section V, we present a brief discussion of related open issues. Section VI concludes the study.

II. INTER-SATELLITE LINKS IN LEO CONSTELLATIONS

The transmission of THz waves in space results in a non-negligible loss in received power, where the distance between the transmitter and receiver is a determining parameter of this loss. This loss is proportional to the square of the distance. Thus, in what follows, we begin by determining the probable distance between the two satellites in both Starlink and Iridium constellations, which are selected as sample networks for this study.

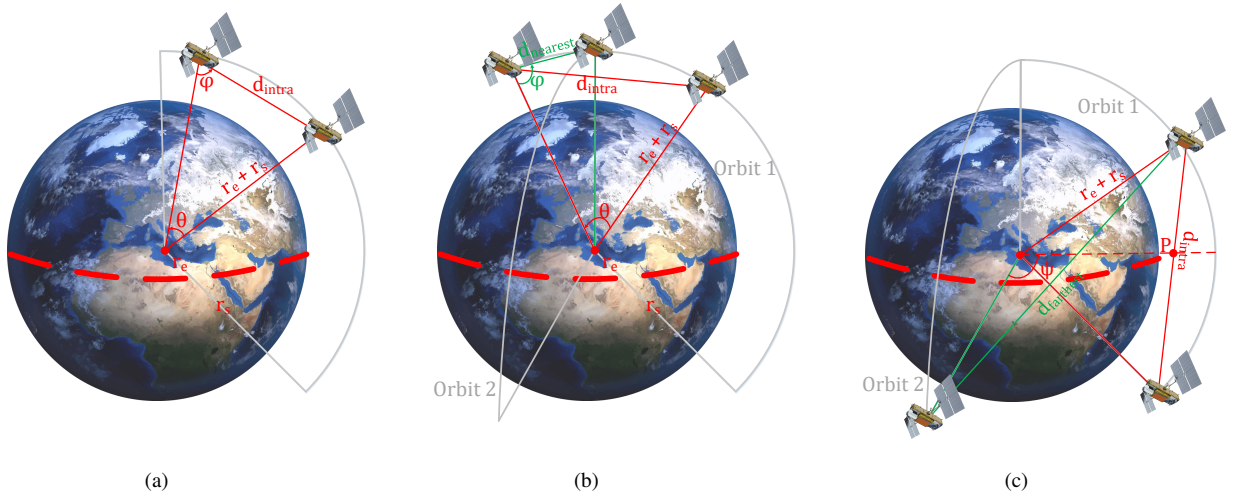


Fig. 2: Satellites can be at various positions—and in various orbits—relative to each other. Three of these distances are: (a) intra-plane distance, (b) the nearest, and (c) the farthest. While the distance between the satellites in the same orbit is constant throughout the movement, the distance between the satellites in the two neighboring orbits changes with time. Two extreme examples of the nearest and farthest are shown.

LEO satellites can be positioned at different distances from each other in different satellite constellations, and some of these distances can be quite significant. The distances between satellites can be investigated in three cases: time-invariant distances between two neighboring satellites in the same orbit (Fig. 2(a)), the nearest distance when one of the satellites is located just over one of the poles (Fig. 2(b)), the farthest distance when one of the satellites is just over the equator (Fig. 2(c)) [22]. Obviously any measure of distance between two satellites in nearby orbits lies in between $d_{nearest}$ and $d_{farthest}$. The first three cases are investigated below. In this study, we only evaluate the analysis for the maximum and minimum distances in order to determine the upper and lower limits of inter-satellite communication performance in terms of error probability. It is clear that the distances between satellites will consist of the values between these two distances. We believe that a performance analysis on the basis of maximum and minimum distances between them constantly changes due to their motion through orbits. Throughout the study, d_{intra} , $d_{nearest}$, and $d_{farthest}$ stand for the inter-satellite distance for an orbit, the shortest and longest distances in between two satellites in nearby orbits, respectively.

A. Intra-plane Distance

The satellites in the same orbit follow each other with the same distance as shown in Fig. 2(a). The distance from the center of the Earth to the satellite, with the Earth radius r_e , is shown by $r_e + r_s$. The angle between two neighboring satellites in the same orbit, $\theta = \frac{360^\circ}{N_{sat}}$, where N_{sat} represents the total number of satellites in the orbit. Since the distances to Earth center are the same for each satellite, the angle between the line from center to satellite and the satellite to satellite line is calculated as

$$\varphi = \frac{180^\circ - \theta}{2}. \quad (1)$$

By using the law of sines, we obtain the following distance:

$$d_{intra} = \frac{(r_e + r_s) \times \sin(\theta)}{\sin(\varphi)}, \quad (2)$$

where d_{intra} and φ denote the distance between two neighboring satellites in the same orbit and the angle between the normal vector and the vector to the neighboring satellite as illustrated in Fig. 2.

B. Inter-plane Distances

In this section, the minimum and maximum distances between satellites in nearby orbits are investigated to reveal the upper and lower limits.

1) *Nearest Distance*: Where two satellites in different orbits are closest to each other, one of the satellites is directly above the north or south pole. It should be noted that, although Starlink satellites do not pass directly over either pole, the north-east orbits form virtual poles above the north and south 53rd-degree latitudes. This scenario is illustrated in Fig. 2(b). Likewise, in the case of intra-plane distance, the nearest distance is found by applying the law of sines as

$$d_{nearest} = \frac{(r_e + r_s) \times \sin(\frac{\theta}{2})}{\sin(\varphi)}, \quad (3)$$

where $\frac{\theta}{2}$ and $\varphi = \frac{180-\theta/2}{2}$ are half of the angle between the line from center of the Earth to satellite and the angle between the inter-satellite line and the line through the center of the Earth, respectively.

2) *Farthest Distance*: When the satellite positions at just over the equator, the distance to the satellite in neighbor orbit becomes maximum as seen in Fig. 2(c). The distance from the center of Earth to the point P is calculated by using Pythagoras theorem as

$$|OP| = \sqrt{(r_e + r_s)^2 - \left(\frac{d_{intra}}{2}\right)^2}. \quad (4)$$

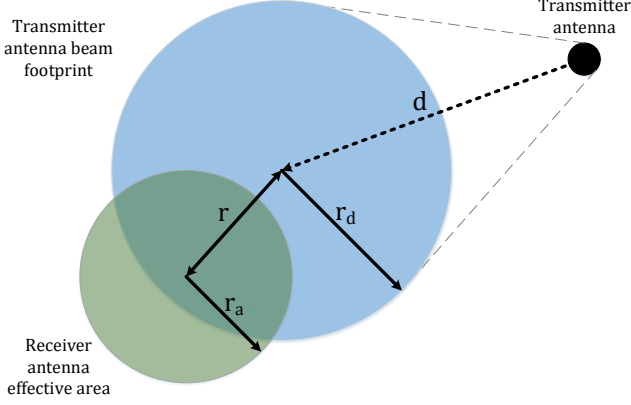


Fig. 3: Illustration of a beam misalignment for the receiver's effective area with radius r_a and the transmitter's beam footprint at distance d shown by r_d with the presence of the pointing error r .

Then, the distance between the satellite in Orbit 2 and the point P is

$$d_{SP} = \sqrt{(r_e + r_s)^2 + |OP|^2 - 2(r_e + r_s)|OP|\cos(\Psi)} \quad (5)$$

where Ψ is the angle between two nearby orbits. Therefore, Ψ is equal to $\frac{180^\circ}{N_{\text{orbit}}}$ for a constellation with N_{orbit} orbits. Finally, the farthest distance between satellites is deduced as

$$d_{\text{farthest}} = \sqrt{d_{SP}^2 + \left(\frac{d_{\text{intra}}}{2}\right)^2}. \quad (6)$$

As an example, the distances are shown in Table I for the two satellite constellations considered in this study: Starlink and Iridium. Since Starlink has more orbits and satellites per orbit, the distances are relatively short compared to the Iridium satellite network.

III. RIS-ASSISTED TERAHERTZ WIRELESS COMMUNICATION IN INTER-SATELLITE LINKS

In this section, RIS-assisted THz ISLs are considered with a misalignment fading due to the sharp beams of THz antennas and the high relative velocity of LEO satellites. To the best of our knowledge, this study is the first to provide an error performance analysis for RIS-assisted THz ISLs in LEO satellite networks.

A. Misalignment Fading

It should be noted that THz antennas create pencil sharp beams. Also, the motion of LEO satellites with high velocity around 28×10^3 kph. Thus, the possible misalignment fading should be considered in THz-empowered ISLs. Under the circular beam assumption, considering beams with the radial distance, r , between their centers on the x-y plane, the misalignment coefficient ζ can be expressed as [23]

$$\zeta(r; d) \approx A_o \exp\left(-\frac{2r^2}{w_{eq}^2}\right), \quad (7)$$

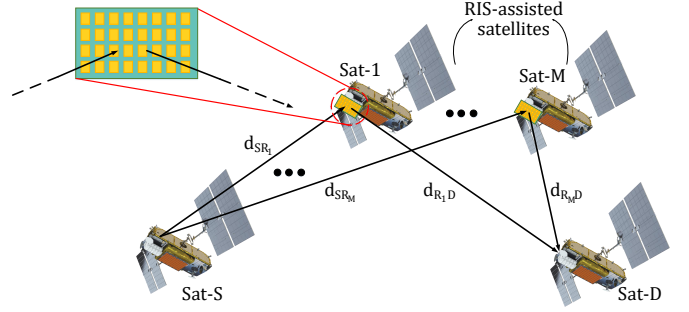


Fig. 4: Illustration of a simultaneous multiple RIS-assisted satellite communication framework consisting of a source (Sat-S), destination (Sat-D), and M satellites equipped with RIS.

where

$$A_0 = \left[\text{erf}\left(\frac{\sqrt{\pi}r_a}{\sqrt{2}r_d}\right) \right]^2, \quad (8)$$

$$w_{eq}^2 = r_d^2 \frac{\text{erf}\left(\frac{\sqrt{\pi}r_a}{\sqrt{2}r_d}\right)}{\frac{\sqrt{2}r_a}{r_d} \exp\left(-\frac{\pi r_a^2}{2r_d^2}\right)}.$$

$\text{erf}(\cdot)$ is the error function. A_0 , w_{eq} , and r_d denote the collected power fraction in the aligned case (i.e., $r = 0$), equivalent beam width, and the beam waist at distance d , respectively. r_a is the radius of the receiver antenna's effective area, which under the circular area assumption can be expressed by modifying the antenna aperture area equation [24] as follows:

$$A_e = \pi r_a^2 = \frac{\lambda^2}{4\pi} G, \quad (9)$$

then,

$$r_a = \frac{\lambda}{2\pi} \sqrt{G}, \quad (10)$$

where G denotes the antenna gain. Due to the fact that the displacement in both directions follows independent identical Gaussian distribution, the radial distance, r , can be modeled by the following Rayleigh distribution:

$$f_r(r) = \frac{r}{\sigma_s^2} \exp\left(-\frac{r^2}{2\sigma_s^2}\right), \quad r > 0, \quad (11)$$

where σ_s^2 stands for the receiver's jitter variance. By jointly utilizing (7) and (11), the misalignment fading is introduced as follows:

$$f_\zeta(y) = \frac{\kappa^2}{A_0^{\kappa^2}} y^{\kappa^2-1}, \quad 0 \leq y \leq A_0, \quad (12)$$

where $\kappa = \frac{w_{eq}^2}{2\sigma_s^2}$ [25]. Thus, the jitter variance appears as an important parameter affecting communication performance.

B. Single RIS-Assisted Wireless Channel and Associated Performance Analysis

Under the flat fading assumption, the signal received by the destination node for N -element RIS is expressed as follows:

$$r = \sqrt{P_t P_L} \left(\sum_{i=1}^N \rho_i^{SR} e^{j\phi_i} \rho_i^{RD} \zeta_i^{SR} \zeta_i^{RD} \right) x + n, \quad (13)$$

where ρ_i^{SR} and ρ_i^{RD} denote the channel coefficients. The phase shift adjusted by the i th element of RIS is represented by ϕ_i . x is the data symbol from possible constellation of an M -ary phase shift keying (PSK) or quadrature amplitude modulation (QAM). n is zero-mean complex additive white Gaussian noise (AWGN) with variance of N_0 . ϕ_i refers to the adjustable phase shifts created by the i^{th} -elements of RIS. ζ_i^{SR} and ζ_i^{RD} stand for the misalignment fading in the links source-to-RIS and RIS-to-destination. Also, P_t and P_L refer to the transmit power of source and the total path loss through the path propagating by the signal, respectively. The total path length is $d_{SR}^2 + d_{RD}^2$ in the near-field behavior; however, it becomes $d_{SR}^2 \times d_{RD}^2$ under the far-field of RIS [26]. The path loss in the free-space is expressed as follows:

$$P_L = \left(\frac{\lambda}{4\pi}\right)^4 \frac{G_i G_r}{d_{SR}^2 d_{RD}^2} \epsilon_p, \quad (14)$$

where G_i and G_r refer to gains in the direction of the incoming and receiving waves, which are chosen as 30 dBi for 350 GHz operating frequency as given in [27]. λ denotes the wavelength corresponding to propagation frequency of wave, ϵ_p stands for the efficiency of RIS. For the lossless RIS, ϵ_p is equal to 1.

By rewriting the channel impulse responses in terms of channel amplitudes and phases as $\rho_i^{SR} = \alpha_i^{SR} e^{-j\beta_i^{SR}}$ and $\rho_i^{RD} = \alpha_i^{RD} e^{-j\beta_i^{RD}}$, Eq. (15) can be expressed as follows:

$$r = \sqrt{P_t P_L} \left(\sum_{i=1}^N \alpha_i^{SR} \alpha_i^{RD} e^{j(\phi_i - \beta_i^{SR} - \beta_i^{RD})} \zeta_i^{SR} \zeta_i^{RD} \right) x + n. \quad (15)$$

Then, the instantaneous signal-to-noise ratio (SNR) observed at the receiver becomes

$$\gamma = \frac{P_t \left| \sqrt{P_L} \left(\sum_{i=1}^N \alpha_i^{SR} \alpha_i^{RD} e^{j\psi} \zeta_i^{SR} \zeta_i^{RD} \right) \right|^2}{N_0}, \quad (16)$$

where $\psi = \phi_i - \beta_i^{SR} - \beta_i^{RD}$ and it is zero for the maximum instantaneous SNR as

$$\gamma_{\max} = \frac{P_t \left| \sqrt{P_L} \left(\sum_{i=1}^N \alpha_i^{SR} \alpha_i^{RD} \zeta_i^{SR} \zeta_i^{RD} \right) \right|^2}{N_0} = \frac{A^2 P_t}{N_0}, \quad (17)$$

where α_i^{SR} and α_i^{RD} follow the Rician distribution which may be observed in the space communication due to the presence of solar scintillation [28] or a high power line of sight (LOS) link with non-line of sight (NLOS) links reflected from other space things. As described in [29], solar scintillation can be modeled with Rician fading. ζ_i^{SR} and ζ_i^{RD} are the misalignment fading coefficients following the distribution given in Eq. (12). According to the central limit theorem (CLT), A follows a Gaussian distribution for $N \gg 1$ with the mean and variance given in (18), where $L_{1/2}(\cdot)$ stands for the Laguerre polynomial of degree 1/2. As A follows a Gaussian distribution, SNR is non-central chi-square distributed with one degree of freedom. To evaluate the bit error probability (BEP), the moment generating function (MGF) of a non-central chi-square distribution [30] is utilized as given in (19). By utilizing the symbol error probability (SEP) expression

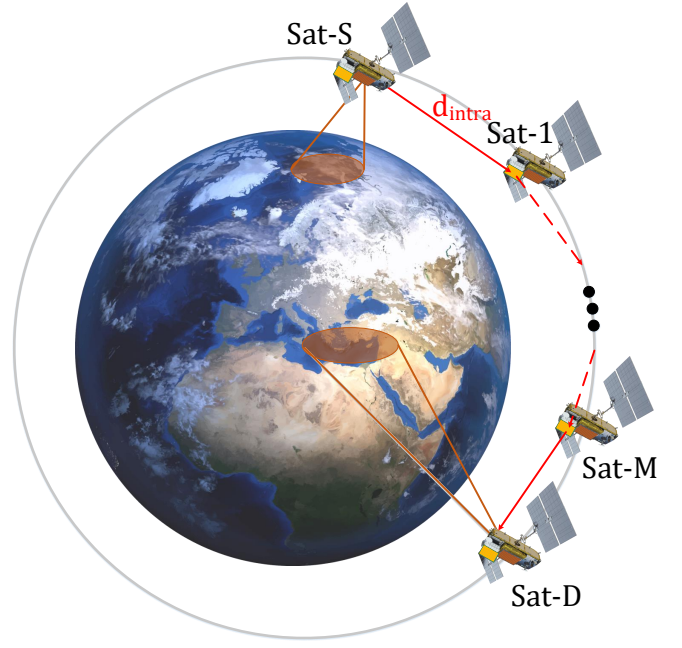


Fig. 5: Illustration of a consecutive multiple RIS-assisted satellite communication framework consisting of a source (Sat-S), destination (Sat-D), and M satellites equipped with RIS, which are in the same orbit.

for M -PSK signals given in [31], the error probability for binary phase shift keying (BPSK) is obtained as in (20). This means that the error probability degrades inversely N^2 while it proportionally increases with $(\sigma_s^2)^4$ due to the term κ in the equation.

C. Multiple RIS-Assisted Wireless Channel and Associated Performance Analysis

In this section, we investigate the performance of the multiple RIS-assisted satellite networks. First, like in [21], we derive a mathematical expression of the error probability for a simultaneous transmission over M independent RISs. Then, we analyze the error performance for the transmission path consisting of M reflections over consecutive RISs.

1) Simultaneous Transmission over M Independent RISs:

For the scenario depicted in Fig. 4, the received signal can be expressed as follows:

$$r = \sqrt{P_t} \left[\sum_{k=1}^M \sqrt{P_{Lk}} \left(\sum_{i=1}^{N_k} \alpha_i^{SRk} \alpha_{i,k}^{RkD} e^{j\psi_k} \zeta_{i,k}^{SRk} \zeta_{i,k}^{RkD} \right) \right] x + n, \quad (21)$$

where each element of Eq. (21) is the same as in Eq. (15) for the k -th RIS. Similar to Eq. (17), the maximum instantaneous SNR is given as follows:

$$\begin{aligned} \gamma_{\max} &= \frac{P_t \left| \sum_{k=1}^M \left[\sqrt{P_{Lk}} \left(\sum_{i=1}^{N_k} \alpha_{i,k}^{SRk} \alpha_{i,k}^{RkD} \zeta_{i,k}^{SRk} \zeta_{i,k}^{RkD} \right) \right] \right|^2}{N_0} \\ &= \frac{A^2 P_t}{N_0}. \end{aligned} \quad (22)$$

$$\begin{aligned}\mathbb{E}[A] &= \frac{N\sqrt{P_L}}{2(1+K)} \frac{\pi}{2} (L_{1/2}(-K))^2 \frac{\kappa^4}{(\kappa^2+1)^2} A_0^2, \\ \text{Var}[A] &= NP_L \left(A_0^4 \frac{\kappa^4}{(\kappa^2+2)^2} - \left[\frac{\pi}{4(1+K)} (L_{1/2}(-K))^2 \frac{\kappa^4}{(\kappa^2+1)^2} A_0^2 \right]^2 \right)\end{aligned}\quad (18)$$

$$M_{\gamma_{\max}}(s) = \frac{\exp\left(-\frac{\frac{P_t}{N_0} \frac{N^2 P_L \pi^2}{16(1+K)^2} (L_{1/2}(-K))^4 \frac{\kappa^8}{(\kappa^2+1)^4} A_0^4}{1-2s \frac{P_t}{N_0} NP_L \left(\frac{A_0^4 \kappa^4}{(\sigma^2+2)^2} - \left[\frac{\pi}{4(1+K)} (L_{1/2}(-K))^2 \frac{\kappa^4}{(\kappa^2+1)^2} A_0^2\right]^2\right)}\right)}{\sqrt{1-2s \frac{P_t}{N_0} NP_L \left(\frac{A_0^4 \kappa^4}{(\kappa^2+2)^2} - \left[\frac{\pi}{4(K+1)} (L_{1/2}(-K))^2 \frac{\kappa^4}{(\kappa^2+1)^2} A_0^2\right]^2\right)}}.\quad (19)$$

$$P_e = \frac{1}{\pi} \int_0^{\pi/2} \frac{\exp\left(-\frac{\frac{P_t}{N_0} \frac{N^2 P_L \pi^2}{16(1+K)^2} (L_{1/2}(-K))^4 \frac{\kappa^8}{(\kappa^2+1)^4} A_0^4}{1+2\sin^2(\omega) \frac{P_t}{N_0} NP_L \left(\frac{A_0^4 \kappa^4}{(\sigma^2+2)^2} - \left[\frac{\pi}{4(1+K)} (L_{1/2}(-K))^2 \frac{\kappa^4}{(\kappa^2+1)^2} A_0^2\right]^2\right)}\right)}{\sqrt{1+2\sin^2(\omega) \frac{P_t}{N_0} NP_L \left(\frac{A_0^4 \kappa^4}{(\kappa^2+2)^2} - \left[\frac{\pi}{4(K+1)} (L_{1/2}(-K))^2 \frac{\kappa^4}{(\kappa^2+1)^2} A_0^2\right]^2\right)}} d\omega.\quad (20)$$

By taking CLT into account for $N_k \gg 1, \forall k = 1, 2, \dots, M$, it can be said that A follows a Gaussian distribution with the mean and variance given as in Eq. (23). Similar to the single RIS-assisted communication performance analysis, we can derive the error probability as stated in Eq. (24), which implies that the error performance increases in proportion to the square of the total reflective elements as given in [21].

2) *Transmission over M Consecutive RIS-Assisted Satellites*: The double-RIS reflected transmission proposed in [21] is generalized for M consecutive RIS reflections as depicted in Fig. 5. Considering the baseband equivalent received signal given in [21], we can generalize the received signal passing through a path consisting of M consecutive RIS reflections as follows:

$$r = \sqrt{P_t P_L} \left[\sum_{i_1=1}^N \sum_{i_2=1}^N \cdots \sum_{i_M=1}^N \alpha_{i_1 \dots i_M} e^{j\psi} \right] x + n, \quad (25)$$

where $\alpha_{i_1 \dots i_M}$ and ψ denote the overall channel amplitude and overall channel phase along with the reconfiguration phases of RISs. It should be noted that the transmitter and receiver are fully aligned in this case. Configuring $\psi = 0$, the maximum instantaneous SNR is obtained as follows:

$$\begin{aligned}\gamma_{\max} &= \frac{P_t \left| \sqrt{P_L} \left[\sum_{i_1=1}^N \sum_{i_2=1}^N \cdots \sum_{i_M=1}^N \alpha_{i_1 \dots i_M} \right] \right|^2}{N_0} \\ &= \frac{A^2 p_t}{N_0}.\end{aligned}\quad (26)$$

For $N \gg 1$, A follows a Gaussian distribution with the mean and variance given below

$$\begin{aligned}\mathbb{E}[A] &= \frac{N^M \sqrt{P_L \pi}}{\sqrt{4(1+K)}} L_{1/2}(-K), \\ \text{Var}[A] &= N^M P_L \left(1 - \frac{\pi}{4(1+K)} (L_{1/2}(-K))^2 \right).\end{aligned}\quad (27)$$

By applying the same procedure as in Section III-C1, the error probability is obtained as follows:

$$P_e = \frac{1}{\pi} \int_0^{\pi/2} \frac{\exp\left(-\frac{\frac{N^{2M} P_L \pi}{4(1+K) L_{1/2}^2(-K)}}{1+2 \frac{N^M P_L}{\sin^2(\omega)} \left(1 - \frac{\pi}{4(1+K)} L_{1/2}^2(-K)\right)}\right)}{\sqrt{1+2 \frac{N^M P_L}{\sin^2(\omega)} \left(1 - \frac{\pi}{4(1+K)} L_{1/2}^2(-K)\right)}} d\omega.\quad (28)$$

IV. NUMERICAL RESULTS AND DISCUSSION

In this section, we present numerical results to support the theoretical findings of Section III. It should be noted that for the simulations in this section, the operating frequency of the system has been set to 350 GHz. The antenna gain is chosen as 30 dBi as given in [27]. As mentioned above, the channel amplitude coefficients follow a Rician distribution with parameter $K = 10$. First of all, we investigate the error performance for single RIS-assisted satellite constellations. Then, multiple RISs are employed in the satellite networks, and the communication performance analyses are carried out regarding these scenarios.

A. Single RIS-Assisted THz Inter-Satellite Links

First, THz ISLs with a single RIS are considered, as depicted in Fig. 1. In this case, there is no direct link between

$$\mathbb{E}[A] = \left(\sum_{k=1}^M N_k \sqrt{P_{Lk}} \right) \times \frac{\pi}{4(1+K)} (L_{1/2}(-K))^2 \frac{\kappa^4}{(\kappa^2+1)^2} A_0^2,$$

$$\text{Var}[A] = \left(\sum_{k=1}^M N_k P_{Lk} \right) \times \left(A_0^4 \frac{\kappa^4}{(\kappa^2+2)^2} - \left[\frac{\pi}{4(1+K)} (L_{1/2}(-K))^2 \frac{\kappa^4}{(\kappa^2+1)^2} A_0^2 \right]^2 \right) \quad (23)$$

$$P_e = \frac{1}{\pi} \int_0^{\pi/2} \frac{\exp \left(- \frac{(\sum_{k=1}^M N_k \sqrt{P_{Lk}})^2 \frac{P_t}{N_0} \frac{\pi^2}{16(1+K)^2} (L_{1/2}(-K))^4 \frac{\kappa^8}{(\kappa^2+1)^4} A_0^4}{1+2 \sin^2(\omega) \frac{P_t}{N_0} (\sum_{k=1}^M N_k P_{Lk}) \left(\frac{A_0^4 \kappa^4}{(\kappa^2+2)^2} - \left[\frac{\pi}{4(1+K)} (L_{1/2}(-K))^2 \frac{\kappa^4}{(\kappa^2+1)^2} A_0^2 \right]^2 \right)} \right)}{\sqrt{1+2 \sin^2(\omega) \frac{P_t}{N_0} (\sum_{k=1}^M N_k P_{Lk}) \left(\frac{A_0^4 \kappa^4}{(\kappa^2+2)^2} - \left[\frac{\pi}{4(K+1)} (L_{1/2}(-K))^2 \frac{\kappa^4}{(\kappa^2+1)^2} A_0^2 \right]^2 \right)}} d\omega. \quad (24)$$

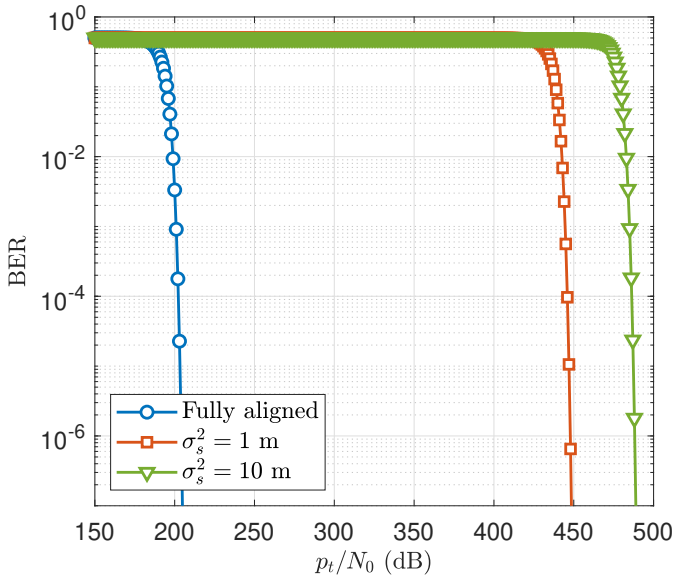


Fig. 6: Bit error rate (BER) performance of a single RIS-assisted Starlink constellation with BPSK signaling over 1024-element RIS for fully aligned transmission and transmission with misalignment jitter.

the source and destination satellites, which is an acceptable assumption considering the satellite constellations [4]. Due to fast relative velocities and possible beam tracking errors, misalignment fading has to be considered. Hence, in this section, misalignment fading is investigated for RIS-assisted THz satellite networks. To the best of our knowledge, this study is the first to consider the misalignment fading in RIS-assisted THz communications.

Two satellite constellations, Starlink and Iridium, are considered as examples, and numerical results are given for these satellite network constellations. Basically, the differences between these two constellations result from the number of orbits and satellites in each orbit. These differences are tabulated in Table I.

We assume that the distances Sat-S to Sat-R and Sat-R to Sat-D are equal to d_{intra} ; in other words, we can think of them being in the same orbit. For Starlink, d_{intra} is 945.4

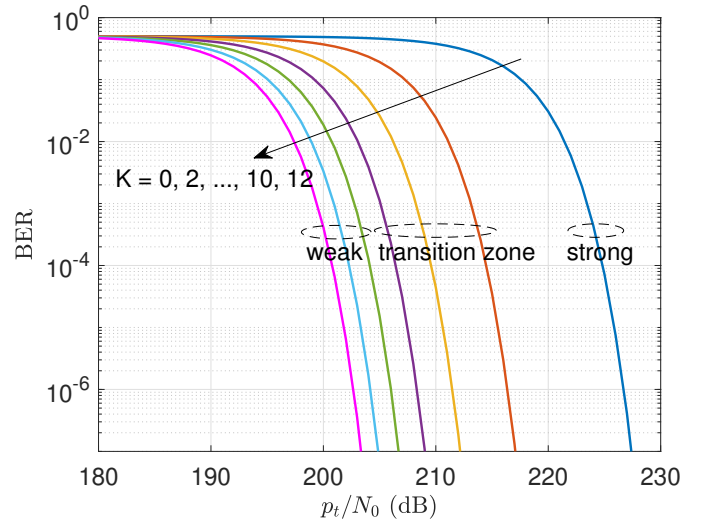


Fig. 7: BER performance of a single RIS-assisted Starlink constellation with BPSK signaling over 1024-element RIS with a changing solar scintillation which shows its effect as the Rician fading on the signal.

km while Iridium's intra-satellite distance is 4034 km. First, the impact of misalignment fading on the error performance is analyzed by comparing a fully aligned system with some jitter variances. Fig. 6 reveals that in parallel with [32], alignment appears to be critical for THz communication systems.

Eq. (20) shows that the jitter variance affects the probability of error in $\frac{\kappa^4}{(\kappa^2+1)^2}$ expression. Since there is a relationship similar to the reverse sigmoid function between the error probability and σ_s , $\frac{\kappa^4}{(\kappa^2+1)^2}$ converges to its minimum value for small values of σ_s . The beginning of this convergence starts around $\sigma_s^2 = 1 \text{ m}^2$. In this study, since $\sigma_s^2 < 1 \text{ m}^2$ values cause almost similar error probability, no analysis is included for a jitter variance less than 1 m^2 . An increase in the variance jitter degrades the error performance until the jitter variance reaches the point where $\frac{\kappa^4}{(\kappa^2+1)^2}$ converges its maximum. Because of the long distances involved, a jitter variance of up to 10 m^2 is considered. Since a jitter variance greater than this could make communication unfeasible, it is not reasonable to evaluate it

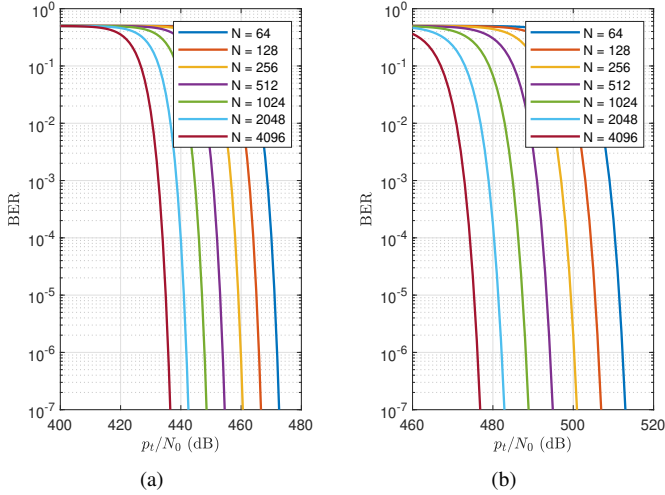


Fig. 8: BER performance of a single RIS-assisted Starlink for different RIS sizes with BPSK signaling and the misalignment fading with the receiver's jitter variance of (a) $\sigma_s^2 = 1 \text{ m}^2$, (b) $\sigma_s^2 = 10 \text{ m}^2$.

in this study.

In deep space channels, solar scintillation has to be taken into account since it results in fluctuations in the signal envelope. As aforementioned above, it follows a Rician distribution. Since the error rate is almost inversely proportional to the square of the shape parameter of Rician fading. The solar scintillation is investigated for three intensity regions: weak scintillation ($K \geq 7$), transition zone ($7 > K > 0$), and strong scintillation ($K = 0$). The impact of solar scintillation on the error performance is shown in Fig. 7. Strong scintillation appears to significantly reduce communication performance. Although increased solar scintillation reduces error performance, its effects are not as serious as misalignment fading.

For varying number of RIS elements, the error performances are depicted in Fig. 8 for the system resembling Starlink. As we can see, when the number of RIS elements is doubled, 6 dB power is gained to satisfy the same error performance as given in Eq. (20). Also, the misalignment fading is investigated in Fig. 8(a) and Fig. 8(b). First, σ_s^2 is assumed to be 1 m. Considering the results shown in both figures, when the jitter variance is increased 10 times, 40 dB more power must be used to ensure the same error performance as shown in Eq. (20). These results indicate that THz satellite networks should either use RIS with a higher number of elements or beam tracking methods that work with very low errors at the expense of high computational costs must be adopted. Similar behaviors are observed in Fig. 9 for Iridium with a higher path loss since it has longer intra-satellite distances than Starlink. As a result, more output power is needed to compensate for path loss.

B. Multiple RIS-Assisted THz Inter-Satellite Links

Since satellite networks are designed to be densely interconnected, multiple satellites equipped with RISs can be deployed in a cooperative manner. Thus, the diversity order can escalate. To this end, we investigate two different cases. First, we look

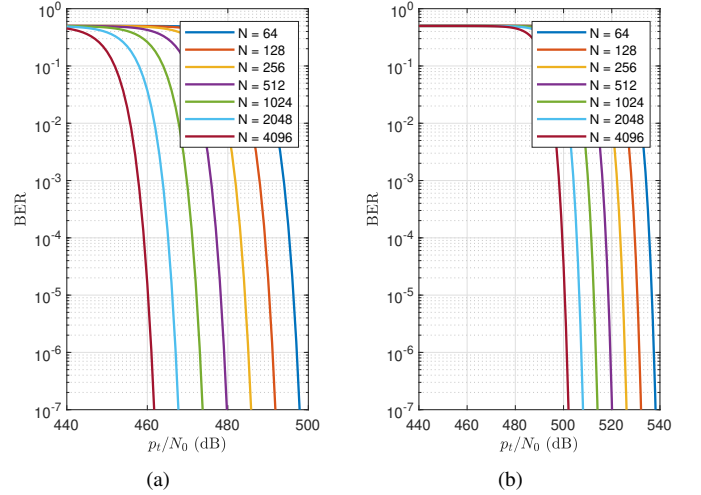


Fig. 9: BER performance of a single RIS-assisted Iridium for different RIS sizes with BPSK signaling and the misalignment fading with the receiver's jitter variance of (a) $\sigma_s^2 = 1 \text{ m}^2$, (b) $\sigma_s^2 = 10 \text{ m}^2$.

at simultaneous transmission over multiple satellites, followed by transmission over M consecutive satellites.

1) *Performance Analysis for Simultaneous Transmission over Multiple Satellites:* As shown in Fig. 4, M satellites equipped with RISs can simultaneously transmit the incident signal to the destination satellite by increasing diversity order and dropping down the path loss exponent [14]. Eq. (24) clearly shows that the error probability is inversely proportional to the square of the total number of RIS elements. It should be noted that in the light of Eq. (24), the misalignment fading remains the same as in a single RIS case. In this scenario, M is selected as 2 with a varying number of RIS elements. It is assumed that each distance is equal to d_{intra} ; hence, $P_{Lk} = P_L, \forall k = 1, 2$. Also, the number of RIS elements is selected as same. In Fig. 10 and Fig. 11, the error performances are investigated for Starlink and Iridium, respectively. In this case, the error rate is proportional to $(2N)^{-2}$. As a result, the same error rate can be achieved with 6 dB less power than the single RIS case.

For the achievable rate analysis, d_{SR_1} and d_{R_1D} is set to d_{intra} . d_{SR_2} and d_{R_2D} vary from $d_{nearest}$ to $d_{farthest}$ to create a scenario such that Sat-S, Sat-1, and Sat-D are consecutive satellites in the same orbit, while Sat-2 is in the nearby orbit. Due to the fact that the positions of the satellites which are in different orbits continuously change and thus, the distance between them fluctuates during their orbits, we evaluate the capacity analysis for the upper and lower limits at the nearest and farthest distances. Fig. 12 and Fig. 13 show achievable rate for Starlink and Iridium satellites equipped with 1024-element RISs for the satellite position between two extreme distances. As expected, the maximum rate is achieved when the distances are minimum. A 10-fold increase in misalignment fading causes the maximum achievable data rate to decrease by 5 bits/s/Hz. For the THz band, this decrease cannot be overlooked since the total data rate decrease reaches

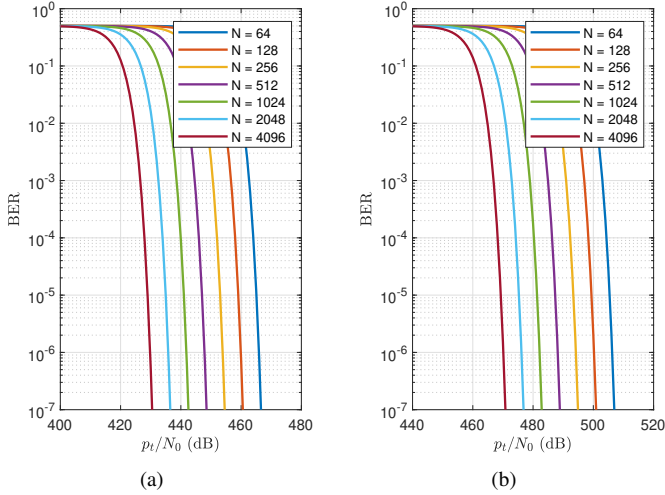


Fig. 10: BER performance of a double simultaneous RIS-assisted Starlink constellation for different RIS sizes with BPSK signaling and a misalignment fading with the receiver's jitter variance of (a) $\sigma_s^2 = 1 \text{ m}^2$ and (b) $\sigma_s^2 = 10 \text{ m}^2$. The distances are assumed as d_{intra} .

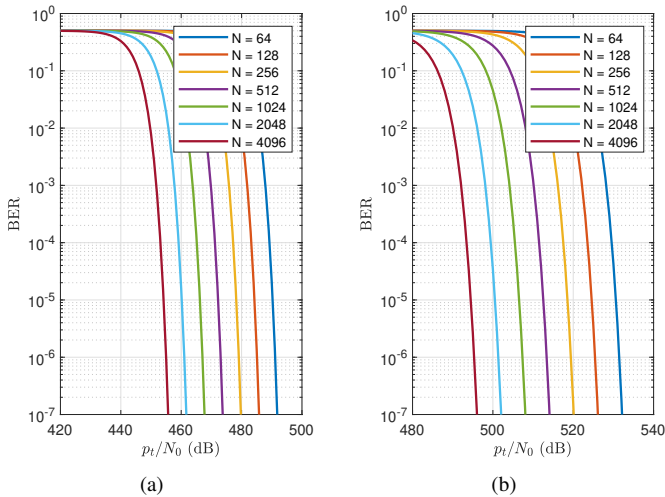


Fig. 11: BER performance of a double simultaneous RIS-assisted Iridium constellation for different RIS sizes with BPSK signaling and a misalignment fading with the receiver's jitter variance of (a) $\sigma_s^2 = 1 \text{ m}^2$ and (b) $\sigma_s^2 = 10 \text{ m}^2$. The distances are assumed as d_{intra} .

300 Gbps for 60 GHz bandwidth. Owing to fact that the path loss between two consecutive satellites in Starlink is less than Iridium network, the achievable rate for Iridium is less. Considering the cost of construction and maintenance of satellites, increasing the number of satellites in each orbit is not feasible. However, increasing the number of RIS elements on each satellite can provide cost-effective solution to reach the desired achievable rate.

2) *Performance Analysis for Transmission over M Consecutive Satellites*: Finally, the transmission sequentially through satellites scenario in the same orbit is investigated because satellite networks are designed to allow communication be-

tween different orbits in a limited way while allowing easy transmission on the same orbit [4]. In this scenario, since all satellites are in the same orbit, the distance between the satellites is constant, so path losses between satellites can be considered equal. It should be noted that the fully aligned case is considered in this scenario.

As Eq. (28) embodies the relation $P_e \propto N^{2M}$, increasing the number of consecutive satellites significantly improves the error performance. For example, increasing from $M = 2$ to $M = 4$ results in approximately 120 dB power gain when 1024-element RISs are employed in satellite networks. The results can be clearly seen in Fig. 14. As we can see there, when the number of RIS elements is doubled, the power gain is 12 dB and 24 dB for $M = 2$ and $M = 4$, respectively. These results indicate that the power gain in transmission along the orbit can increase significantly.

V. OPEN ISSUES

We can observe from the foregoing that satellite-mounted RIS communication systems can increase error probability performance, but there are some open issues. Due to the continuous movement of satellites along their orbits, their positions relative to each other change. Therefore, adaptive and steerable beam antenna designs are clearly needed. In addition, since the orbits of the satellites can be planned and predicted, coarse beam alignment can be performed by utilizing a look-up table of the positions of the other satellites in each satellite. Then, beam steering methods can be used for precise alignment. Furthermore, the derivations in this study show that the system can be less affected by misalignment loss by using antennas with large beamwidths. As discussed in [33–35], it is possible to produce antennas with large beamwidths in the THz region by using semiconductors such as graphene and manufacturing techniques such as micro-machining. Finally, a deeper investigation of solar scintillation in the THz band is needed to improve the accuracy of the performance analysis.

Since the potential of the THz region has only just begun to be explored in terms of communication, THz hardware has yet to reach the desired maturity level. In particular, there is a serious need for amplifier designs for inter-satellite communication links. Still it should be noted that the RIS-supported communication proposed in this study can be used in the lower bands for satellite-to-ground and inter-satellite connections. The derivations indicate that halving the operation frequency can reduce the required power by 12 dB at the cost of a decrease in the achievable rate owing to the presence of the narrowband at lower frequency regions.

Furthermore, a path that can minimize the target performance metrics, such as round trip time, can be investigated by using RISs with an optimization framework. Thus, RISs can be used not only to improve communication performance but also to address other requirements, such as reducing the latency between two nodes. By modeling this problem as a traveling sales man problem, the path satisfying the minimum latency can be solved by mixed integer nonlinear programming. Furthermore, a performance analysis is needed

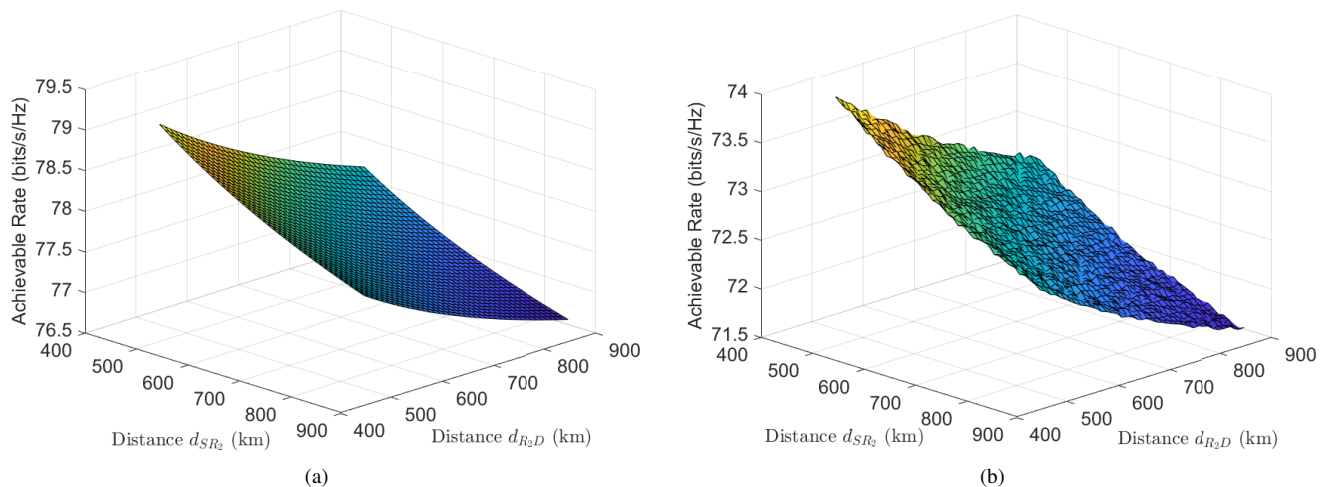


Fig. 12: Achievable data rate performance for the double simultaneous RISs-assisted Starlink constellation for varying distances (i.e., d_{SR_2} and d_{R_2D}) from $d_{nearest}$ to $d_{farthest}$ with two misalignment cases: (a) $\sigma_s^2 = 1 \text{ m}^2$, (b) $\sigma_s^2 = 10 \text{ m}^2$ where $N = 1024$. d_{SR_1} and d_{R_1D} are kept constant as d_{intra} .

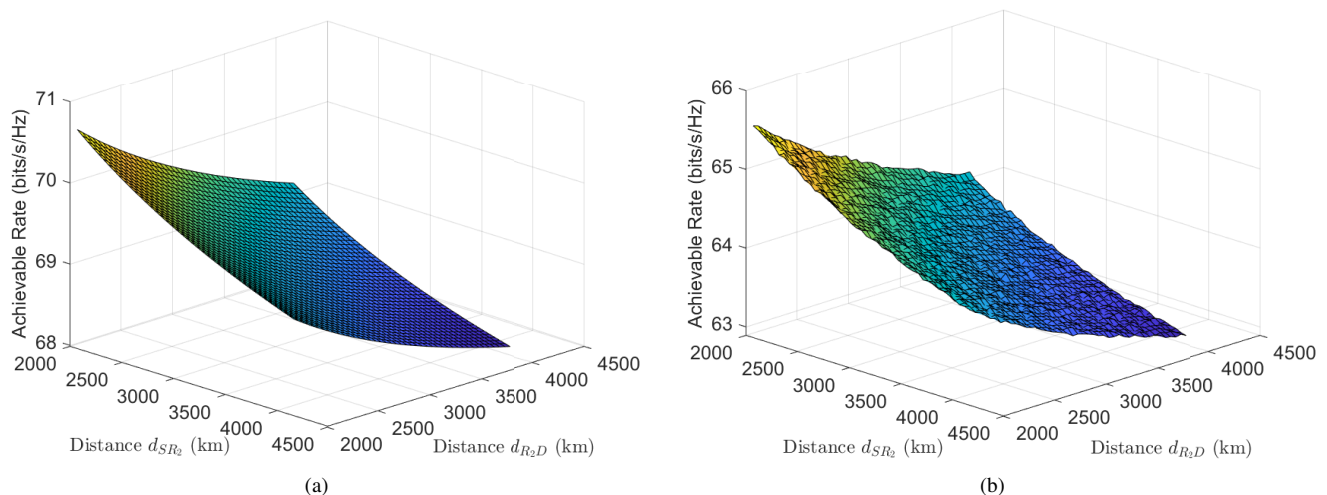


Fig. 13: Achievable data rate performance for the double simultaneous RISs-assisted Iridium constellation for varying distances (i.e., d_{SR_2} and d_{R_2D}) from $d_{nearest}$ to $d_{farthest}$ with two misalignment cases: (a) $\sigma_s^2 = 1 \text{ m}^2$, (b) $\sigma_s^2 = 10 \text{ m}^2$ where $N = 1024$. d_{SR_1} and d_{R_1D} are kept constant as d_{intra} .

for when satellites move through their orbits. This can be obtained by utilizing orbit modeling tools, such as SaVi.

VI. CONCLUSIONS

In this study, a solution to both frequency scarcity and low-complexity system design was proposed by the joint use of RIS and THz band in LEO ISLs. It was shown to be possible to increase achievable rates with the ultra-wide bandwidth provided by the THz wave and the RIS acting like N-elements virtual MIMO system. The derived mathematical expressions and simulation results demonstrated that an increase in the number of RISs can reduce the required transmission power targeting the same error probability. It was also shown that error probability decreases inversely proportional to the square of the number of elements of RIS. Furthermore, we considered the issue of misalignment fading, which can occur in THz LEO

satellite networks and which were validated with simulation results. Our study shows that misalignment between the antennas gives rise to a severe drop in the received power. This indicates that a beam tracker is needed to ensure a convenient alignment system between the antennas. Also, it is shown by both derivations and simulation results that solar scintillation has a significant effect on error performance. In addition, considering the node density of the next-generation LEO satellites networks, cooperative communication techniques has emerged as a promising tool to improve the ISL performances. Finally, we investigated the performance of simultaneous and consecutive transmission between satellites equipped with more than one RIS, which demonstrated that simultaneous and consecutive transmission enhances communication in terms of error probability. Moreover, the achievable rate was simulated for the position of the satellites in space under both the aligned

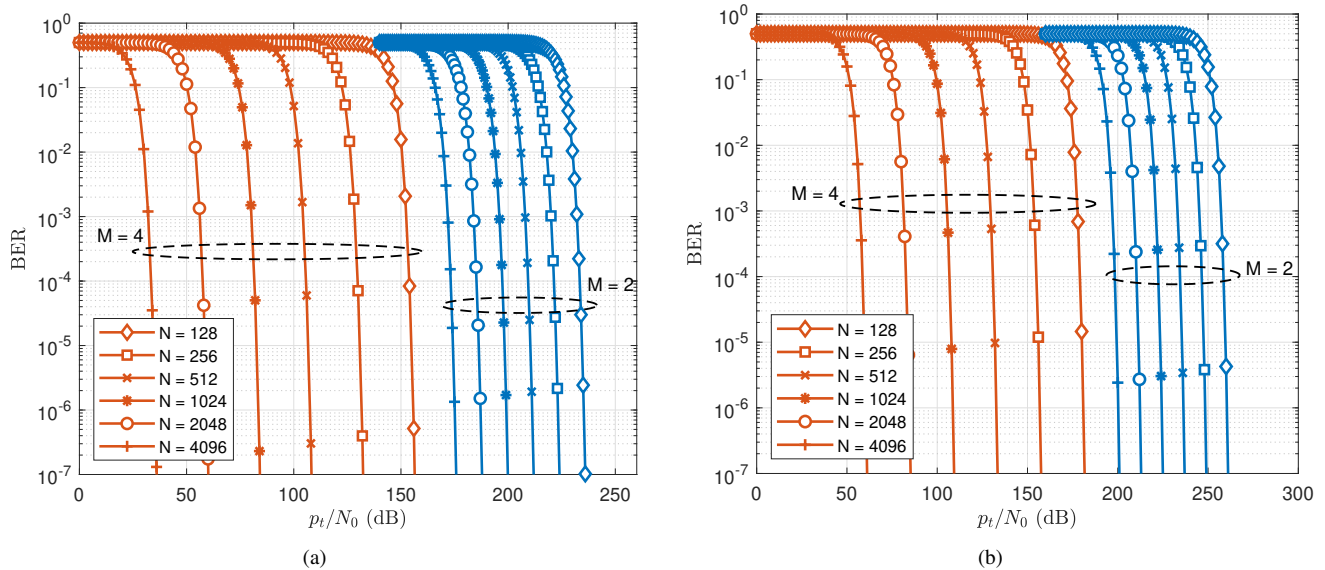


Fig. 14: BER performance for the transmission over consecutive satellites equipped with N -element RIS in two different constellations: (a) Starlink, (b) Iridium. In this case, all satellites are assumed to be in the same orbit; thus, the inter-satellite distance is d_{intra} .

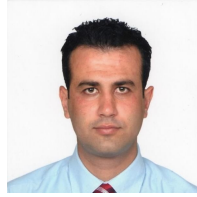
case and misalignment fading.

REFERENCES

- [1] K. Woellert, P. Ehrenfreund, A. J. Ricco, and H. Hertzfeld, "Cubesats: Cost-effective science and technology platforms for emerging and developing nations," *Advances in Space Research*, vol. 47, no. 4, pp. 663–684, 2011.
- [2] N. Saeed, A. Elzanaty, H. Almorad, H. Dahrouj, T. Y. Al-Naffouri, and M.-S. Alouini, "Cubesat communications: Recent advances and future challenges," *IEEE Commun. Surv. Tutorials*, vol. 22, no. 3, pp. 1839–1862, 2020.
- [3] I. F. Akyildiz and A. Kak, "The Internet of space things/CubeSats," *IEEE Network*, vol. 33, no. 5, pp. 212–218, 2019.
- [4] M. Handley, "Delay is not an option: Low latency routing in space," in *Proceedings of the 17th ACM Workshop on Hot Topics in Networks*, 2018, pp. 85–91.
- [5] K. Tekbiyik, A. R. Ekti, G. K. Kurt, A. Gorcin, and H. Yanikomeroglu, "A holistic investigation of terahertz propagation and channel modeling toward vertical heterogeneous networks," *IEEE Commun. Mag.*, vol. 58, no. 11, pp. 14–20, 2020.
- [6] C. Chaccour, M. N. Soorki, W. Saad, M. Bennis, P. Popovski, and M. Debbah, "Seven defining features of terahertz (THz) wireless systems: A fellowship of communication and sensing," *IEEE Commun. Surv. Tutor.*, vol. *Early Access*, pp. 1–27, 2022.
- [7] T. Schneider, A. Wiatrek, S. Preußler, M. Grigat, and R.-P. Braun, "Link budget analysis for terahertz fixed wireless links," *IEEE Trans. Terahertz Sci. Technol.*, vol. 2, no. 2, pp. 250–256, 2012.
- [8] K. Tekbiyik, E. Ulusoy, A. R. Ekti, S. Yarkan, T. Baykaş, A. Görçin, and G. K. Kurt, "Statistical channel modeling for short range line-of-sight terahertz communication," in *30th Annual International Symposium on Personal, Indoor and Mobile Radio Communications (PIMRC)*, 2019, pp. 1–5.
- [9] S. Priebe, M. Jacob, and T. Kürner, "Affection of THz indoor communication links by antenna misalignment," in *6th European Conference on Antennas and Propagation (EUCAP)*, 2012, pp. 483–487.
- [10] A. R. Ekti, A. Boyaci, A. Alparslan, İ. Ünal, S. Yarkan, A. Görçin, H. Arslan, and M. Uysal, "Statistical modeling of propagation channels for terahertz band," in *IEEE Conference on Standards for Communications and Networking (CSCN)*, 2017, pp. 275–280.
- [11] C. Liaskos, S. Nie, A. Tsioliaridou, A. Pitsillides, S. Ioannidis, and I. Akyildiz, "A new wireless communication paradigm through software-controlled metasurfaces," *IEEE Commun. Mag.*, vol. 56, no. 9, pp. 162–169, 2018.
- [12] Q. Wu and R. Zhang, "Towards smart and reconfigurable environment: Intelligent reflecting surface aided wireless network," *IEEE Commun. Mag.*, vol. 58, no. 1, pp. 106–112, 2019.
- [13] E. Arslan, I. Yildirim, F. Kilinc, and E. Basar, "Over-the-air equalization with reconfigurable intelligent surfaces," *arXiv preprint arXiv:2106.07996*, 2021.
- [14] E. Basar, M. Di Renzo, J. De Rosny, M. Debbah, M.-S. Alouini, and R. Zhang, "Wireless communications through reconfigurable intelligent surfaces," *IEEE Access*, vol. 7, pp. 116 753–116 773, 2019.
- [15] E. Basar, "Transmission through large intelligent surfaces: A new frontier in wireless communications," in *Proc. Eur. Conf. Netw. Commun. (EuCNC)*, 2019, pp. 112–117.
- [16] J. Ye, J. Qiao, A. Kammoun, and M.-S. Alouini, "Non-terrestrial communications assisted by reconfigurable intelligent surfaces," *Proc. IEEE*, vol. *Early Access*, pp. 1–43, 2022.
- [17] K. Tekbiyik, G. K. Kurt, and H. Yanikomeroglu, "Energy-efficient RIS-assisted satellites for IoT networks," *IEEE Internet Things J.*, vol. *Early Access*, pp. 1–10, 2021.
- [18] W. U. Khan, E. Lagunas, A. Mahmood, S. Chatzinotas, and B. Ottersten, "When RIS meets geo satellite communications: a new optimization framework in 6G," *arXiv preprint arXiv:2202.00497*, 2022.
- [19] B. Zheng, S. Lin, and R. Zhang, "Intelligent reflecting surface-aided LEO satellite communication: Cooperative passive beamforming and distributed channel estimation," *arXiv preprint arXiv:2201.02913*, 2022.
- [20] M. Handley, "Using ground relays for low-latency wide-area routing in megaconstellations," in *Proceedings of the 18th ACM Workshop on Hot Topics in Networks*, 2019, pp. 125–132.
- [21] I. Yildirim, A. Uyrus, and E. Basar, "Modeling and analysis of reconfigurable intelligent surfaces for indoor and outdoor applications in future wireless networks," *IEEE Trans. on Commun.*, vol. 69, no. 2, pp. 1290–1301, 2021.
- [22] X. Yang, "Low Earth Orbit (LEO) Mega Constellations: Satellite and Terrestrial Integrated Communication Networks," Ph.D. dissertation, University of Surrey, 2019.
- [23] A. A. Farid and S. Hranilovic, "Outage capacity optimization for free-space optical links with pointing errors," *Journal of Lightwave Technology*, vol. 25, no. 7, pp. 1702–1710, Jul. 2007.
- [24] C. A. Balanis, *Antenna Theory: Analysis and Design*. John Wiley & Sons, 2016.
- [25] A.-A. A. Boulogeorgos and A. Alexiou, "Error analysis of mixed THz-RF wireless systems," *IEEE Commun. Lett.*, vol. 24, no. 2, pp. 277–281, Feb. 2020.
- [26] S. W. Ellingson, "Path loss in reconfigurable intelligent surface-enabled channels," in *IEEE 32nd Annual International Symposium on Personal*,

Indoor and Mobile Radio Communications (PIMRC), 2021, pp. 829–835.

- [27] R. Piesiewicz, M. Jacob, M. Koch, J. Schoebel, and T. Kurner, “Performance analysis of future multigigabit wireless communication systems at THz frequencies with highly directive antennas in realistic indoor environments,” *IEEE J. Sel. Top. Quantum Electron.*, vol. 14, no. 2, pp. 421–430, Mar. 2008.
- [28] D. Morabito, “Solar corona amplitude scintillation modeling and comparison to measurements at X-band and Ka-band,” *IPN Progress Report*, vol. 42, no. 153, 2003.
- [29] P. Shaft, “On the relationship between scintillation index and Rician fading,” *IEEE Trans. Commun.*, vol. 22, no. 5, pp. 731–732, 1974.
- [30] J. G. Proakis, *Digital Communications*. 4th ed. New York: McGraw-Hill, 2001.
- [31] M. K. Simon and M.-S. Alouini, *Digital Communication over Fading Channels*. John Wiley & Sons, 2005, vol. 95.
- [32] A.-A. A. Boulogeorgos, E. N. Papasotiriou, and A. Alexiou, “Analytical performance assessment of THz wireless systems,” *IEEE Access*, vol. 7, pp. 11 436–11 453, 2019.
- [33] Y. Luo, Q. Zeng, X. Yan, Y. Wu, Q. Lu, C. Zheng, N. Hu, W. Xie, and X. Zhang, “Graphene-based multi-beam reconfigurable THz antennas,” *IEEE Access*, vol. 7, pp. 30 802–30 808, 2019.
- [34] B. Wu, Y. Hu, Y. T. Zhao, W. B. Lu, and W. Zhang, “Large angle beam steering THz antenna using active frequency selective surface based on hybrid graphene-gold structure,” *Optics Express*, vol. 26, no. 12, pp. 15 353–15 361, 2018.
- [35] A. Gomez-Torrent, M. Garcia-Vigueras, L. Le Coq, A. Mahmoud, M. Ettore, R. Sauleau, and J. Oberhammer, “A low-profile and high-gain frequency beam steering subterahertz antenna enabled by silicon micromachining,” *IEEE Trans. Antennas Propag.*, vol. 68, no. 2, pp. 672–682, 2019.



Ali Rıza Ekti is from Tarsus, Turkey. He received the B.Sc. degree in electrical and electronics engineering from Mersin University, Mersin, Turkey, in June 2006, the M.Sc. degree in electrical engineering from the University of South Florida, Tampa, FL, USA, in December 2009, and the Ph.D. degree in electrical engineering from the Department of Electrical Engineering and Computer Science, Texas A&M University, in August 2015. He was a Visiting Professor at the Electrical and Computer Engineering Department of Gannon University, Erie, PA between August 2015 and June 2016. He worked as an Assistant Professor with the Electrical and Electronics Engineering Department, Balıkesir University and held the Division Manager position of HISAR Laboratory, TÜBİTAK BİLGEM, where he was responsible for research and development activities in the wireless communications and signal processing between November 2016 and December 2021. In January 2022, he joined Grid Communications and Security Research Group, Oak Ridge National Laboratory, Knoxville, TN, USA, where he is currently a Senior R&D Staff Member. His current research interests include statistical signal processing, wireless propagation channel modeling, optimization, machine learning in 5G and beyond systems and anomaly detection in smart grid.

Kürşat Tekbiyık [StM'19] (tekbiiyik@itu.edu.tr) received his B.Sc. and M.Sc. degrees (with high honors) in electronics and communication engineering from Istanbul Technical University, Istanbul, Turkey, in 2017 and 2019, respectively. He is currently pursuing his Ph.D. degree in telecommunications engineering in Istanbul Technical University. His research interests include algorithm design for signal intelligence, next-generation wireless communication systems, terahertz wireless communications, and machine learning.



Halim Yanikomeroğlu [F] (halim@sce.carleton.ca) is a full professor in the Department of Systems and Computer Engineering at Carleton University, Ottawa, Canada. His research interests cover many aspects of 5G/5G+ wireless networks. His collaborative research with industry has resulted in 39 granted patents. He is a Fellow of the Engineering Institute of Canada and the Canadian Academy of Engineering, and he is a Distinguished Speaker for IEEE Communications Society and IEEE Vehicular Technology Society.



Güneş Karabulut Kurt [StM'00, M'06, SM'15] (gkurt@itu.edu.tr) received the Ph.D. degree in electrical engineering from the University of Ottawa, Ottawa, ON, Canada, in 2006. Between 2005 and 2008, she was with TenXc Wireless, and Edgewater Computer Systems, in Ottawa Canada. From 2008 to 2010, she was with Turkcell R&D Applied Research and Technology, Istanbul. Since 2010, she has been with Istanbul Technical University. She is also an Adjunct Research Professor at Carleton University. She is serving as an Associate Technical Editor of



IEEE Communications Magazine.